J Mater Sci (2013) 48:8235–8243
DOI 10.1007/s10853-013-7636-7

Elastic, optoelectronic, and thermal properties of cubic CSi_2N_4: an ab initio study

A. Haddou · H. Khachai · R. Khenata · F. Litimein · A. Bouhemadou · G. Murtaza · Z. A. Alahmed · S. Bin-Omran · B. Abbar

Received: 22 April 2013 / Accepted: 29 July 2013 / Published online: 10 August 2013

Abstract The mechanical, optoelectronic, and thermodynamic properties of carbon silicon nitride spinel compound have been investigated using density functional theory. The exchange–correlation potential was treated with the local density approximation (LDA) and the generalized gradient approximation of Perdew–Burke and Ernzerhof (PBE-GGA). In addition, the Engel–Vosko generalized gradient approximation (EV-GGA) and the modified Becke–Johnson potential (TB-mBJ) were also applied to improve the electronic band structure calculations. The ground state properties, including lattice constants and bulk modulus, are in fairly good agreement with the available theoretical data. The elastic constants, Young's modulus, shear modulus, and Poisson's ratio have been determined by using the variation of the total energy with strain. From the elastic parameters, it is inferred that this compound is brittle in nature. The results of the electronic band structure show that CSi_2N_4 has a direct energy band gap (Γ–Γ). The TB-mBJ approximation yields larger fundamental band gaps compared to those of LDA, PBE-GGA, and EV-GGA. In addition, we have calculated the optical properties, namely, the real and the imaginary parts of the dielectric function, refractive index, extinction coefficient, reflectivity, and energy loss function for radiation up to 40.0 eV. Using the quasi-harmonic Debye model which considers the phononic effects, the effect of pressure P and temperature T on the lattice parameter, bulk modulus, thermal expansion coefficient, Debye temperature, and the heat capacity for this compound were investigated for the first time.

Introduction

The search for new ultra-incompressible superhard materials compared to diamond and cubic boron nitride c-BN has received a considerable effort and remains one of the most dominated areas of the high-pressure research for

A. Haddou · H. Khachai · F. Litimein
Physics Department, Djillali Liabes University of Sidi Bel-Abbes, Sidi Bel Abbès, Algeria

A. Haddou · H. Khachai
Applied Materials Laboratory, Electronics Department, Djillali Liabes University of Sidi Bel-Abbes, Sidi Bel Abbès, Algeria

R. Khenata
Laboratoire de Physique Quantique et de Modélisation Mathématique, Université de Mascara, 29000 Mascara, Algeria
e-mail: khenata_rabah@yahoo.fr

A. Bouhemadou
Laboratory for Developing New Materials and their Characterization, Department of Physics, Faculty of Science, University of Setif, 19000 Setif, Algeria

G. Murtaza (✉)
Materials Modeling Lab, Department of Physics, Islamia College University, Peshawar, Pakistan
e-mail: murtaza@icp.edu.pk

Z. A. Alahmed · S. Bin-Omran
Department of Physics and Astronomy, College of Science, King Saud University, P.O. Box 2455, Riyadh 11451, Saudi Arabia

B. Abbar
Laboratoire de Modélisation et Simulation en Sciences des Matériaux, Physics Department, Djillali Liabès University of Sidi Bel-Abbès, 22000 Sidi Bel Abbès, Algeria

several decades. There is a significant interest on synthesizing and characterization of novel superhard materials showing very low compressibility and large durability [1, 2]. Recently, more attention has been focused on high-pressure (HP) spinel nitrides: γ-Ge_3N_4 and γ-Sn_3N_4 and particularly on γ-Si_3N_4 having cubic Th_3P_4-type structure. The most eminent representative of γ-Si_3N_4 was found to have combined properties of high fracture toughness, hardness and wear resistance, low coefficient of thermal expansion, and relatively high elastic modulus. Thus, silicon nitride can be considered as an excellent material for engine parts or other applications such as bearings and metal machining [3–6]. In optoelectronic applications, Si_3N_4 is used as wide direct band gap semiconductor making it suitable for fabrication of blue LEDs [7, 8].

Extensive researches on this binary cubic spinel nitride Si_3N_4 have emphasized the collaboration between the three methods namely laser-heated diamond anvil cells LH-DAC and multi-anvil techniques and quantum mechanical calculations [3, 5–18]. Particularly, the structure of Si_3N_4 was initially formed by chemical reaction from amorphous and crystalline Si_3N_4 at high pressures ($\sim$15 GPa) and high temperatures ($\sim$2200 K) where the mechanical properties were determined both by in situ synchrotron experiments, and by indentation studies of recovered samples [19–22]. A computational study performed by Wang and co-workers [25] indicated high bulk (300 GPa) and shear moduli (340 GPa) for γ-Si_3N_4, while it predicted the hardness of γ-Si_3N_4 to be close to the experimental value (33 GPa) as in Ref. [9] and demonstrated that γ-Si_3N_4 is not actually a superhard material [22]. Subsequently, some systematic investigations have been extended to improve the elastic properties of the pure γ-Si_3N_4 so that various structural changes have been studied by replacing C with Si or Ge atoms in the conventional A_3N_4 structure. The proposed structure γ-CSi_2N_4 was predicted to have a good mechanical stability with a relatively big elastic constant [6, 22–25]. Recently using the microscopic model of hardness, γ-CSi_2N_4 was expected to be a superhard material with obtained hardness value of 52.07 GPa, while the hardness of γ-Si_3N_4 is 33.3 GPa [26]. Therefore, ternary nitride spinel can be viewed as excellent candidates for low compressibility materials, or at least as precursors for super hard polymorph.

In view of the promising technological applications of γ-CSi_2N_4 we see that there is a dearth of experimental and theoretical information on this ternary cubic nitride alloy [27–29]. Several efforts have been focused on investigating the structural, elastic, and electronic properties of this compound [6, 23–26, 30]. The optical properties, or more specifically the complex dielectric functions, of γ-CSi_2N_4 have been addressed by Wang et al. [25] by means of ab initio electronic structure calculations via the linearized augmented planes wave (LAPW) method. To the best of our knowledge, no thermal properties of γ-CSi_2N_4 compound have been reported in literature. Therefore, it motivates us to deal with the thermal properties of γ-CSi_2N_4 in the present paper.

The rest of the paper is divided in to three parts. In "Calculation details" section, we briefly describe the computational techniques used in this study. In "Results and discussion" section, the most relevant results obtained for the structural, elastic, electronic, optical, and thermodynamic properties of γ-CSi_2N_4 compound are presented and compared with previous theoretical calculations when available. "Conclusions" section summarizes the main conclusions of our work.

Calculation details

Calculations were carried out with APW + lo method [31] based on the density functional theory (DFT) [32, 33] as implemented in the WIEN2K code [34]. The APW + lo method expands the Kohn–Sham orbitals in atomic like orbitals inside the muffin-tin (MT) atomic spheres and plane waves in the interstitial region. The exchange–correlation potential was treated with the PW-LDA and PWE-GGA approximations. Moreover, the Engel–Vosko generalized gradient approximation (EV-GGA) formalism [35] and the recent modified Becke–Johnson potential (TB-mBJ) [36] were also applied to improve the electronic band structure and optical properties. Such approximations have been demonstrated to be very good in predicting band gap energies of bulk materials. A plane-wave cutoff parameter $R_{MT}K_{max}$ of 8 was used (where R_{MT} is the minimum radius of the muffin-tin spheres and K_{max} gives the magnitude of the largest k-vector in the plane wave expansion). The atomic sphere radii of the atoms were taken as large as possible without overlap between the spheres: 2.0, 1.4, and 2.1 a.u. for C, N, and Si, respectively. The spherical harmonics inside the muffin-tin spheres are expanded up to $l_{max} = 10$, while the Fourier expanded charge density was truncated at $G_{max} = 12$ (a.u.)$^{-1}$. The self-consistent calculations are considered to be converged when the total energy of the system is stable within 10^{-4} Ry. The integrals over the Brillouin zone (IBZ) are performed with 47 k-points using the Monkhorst–Pack special k-points approach [37].

In general, the optical properties of the matter may be derived from the knowledge of the complex dielectric function $\varepsilon(\omega) = \varepsilon_1(\omega) + i\varepsilon_2(\omega)$. The imaginary part $\varepsilon_2(\omega)$ was obtained directly from the FLAPW electronic structure calculations, while the real part $\varepsilon_1(\omega)$ is obtained through the use of the familiar Kramers–Kronig relation [38]. All the other optical constants, such as the refractive index

$n(\omega)$, the extinction coefficient $k(\omega)$, the optical reflectivity $R(\omega)$, and the energy-loss spectrum $L(\omega)$, can be computed from the values of $\varepsilon(\omega)$ [39, 40]. For the calculation of the optical properties, which usually requires a dense mesh of uniformly distributed k-points, the BZ integration was performed using a 20 × 20 × 20 MP k-mesh.

The investigations of thermal effects in this study are performed within the quasiharmonic Debye theory of crystals to overcome the extensive and complicated lattice dynamics calculations. We apply here the quasi-harmonic Debye model, implemented in the pseudo code Gibbs [41]. Debye model is developed for crystalline solids. In a typical calculation, from an energy–volume (E–V) data obtained from APW + lo method, the Gibbs program allows us to evaluate the Debye temperature to obtain the Gibbs free energy $G(V, P, T)$ and to minimize G for deriving the thermal equation of state (EOS) $V(P, T)$. Other macroscopic properties related to the pressure (P) and temperature (T) can be obtained by using some standard thermodynamic relations. Further details of this procedure can be found elsewhere [41].

Results and discussion

Structural and elastic properties

The general formula for spinel compounds is AB_2X_4, where A and B represent the cations and X the anions. The spinel unit cell is face-centered cubic with Fd-3m (No. 227) space group including eight formula units. Among the 56 atoms included in the unit cell, the 32 X anions lie on the 32e (u, u, u) sites, while 8 cations are in the tetrahedral (8a) (1/8, 1/8, 1/8) sites and 16 cations are in the octahedral (16c) (1/2, 1/2, 1/2) sites [22]. The crystalline structure is characterized by two parameters not fixed by the symmetry: the lattice parameter a and the internal free parameter u defining the position of the X atoms. The value of the internal free parameter u lies between 0.24 and 0.275 if the origin of the unit cell is taken at the center of inversion.

The ground state properties such as the equilibrium lattice constant a, the bulk modulus B, and its pressure derivative B' are determined by fitting the calculated total energies versus unit cell volume curve shown in Fig. 1 to the Murnaghan's EOS [42]

$$E(V) = E_0 + \frac{B}{B'(B'-1)}\left[V\left(\frac{V_0}{V}\right)^{B'} - V_0\right] + \frac{B}{B'}(V - V_0).$$

The calculated structural parameters of γ-CSi_2N_4 within LDA and GGA approximations together with other theoretical and experimental values are summarized in Table 1.

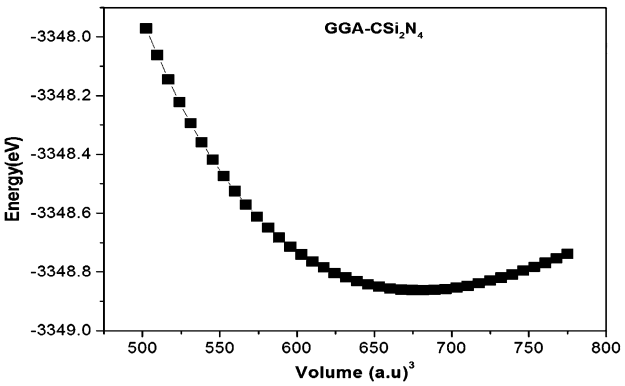

Fig. 1 The variation of total energy with unit cell volume for γ-CSi_2N_4 using GGA approximation

Table 1 Calculated lattice constant a (in Å), nitride free internal parameter u, bulk modulus B (in GPa), pressure derivative B' of γ-CSi_2N_4 within the LDA and the GGA approximations together with other theoretical calculations

Properties	Present work		Other
	LDA	GGA	
a	7.3854	7.2883	7.4044[a], 7.2737[b], 7.3514[c], 7.32–7.5209[d]
u	0.2496	0.2494	
B	341.03	374.48	329.7[a], 342.6[b], 349.9[c], 309.5–344[d]
B'	3.83	3.94	4.26[a], 3.82[c]

[a] Ref. [25]
[b] Ref. [26]
[c] Ref. [30]
[d] Ref. [6, 24]

There is a good agreement between our results and those of the previous calculations.

Progress in ab initio calculation enables to study the mechanical properties and can provide more fundamental insight into the true, namely atomistic, mechanisms of fracture. A cubic crystal has three independent single-crystal elastic constants, namely, C_{11}, C_{12}, and C_{44}. They can be determined by applying a small strain to the equilibrium lattice and computing the resultant change in its total energy with preserved volume [43]. Our calculated elastic constants of γ-CSi_2N_4 at $P = 0$ GPa and $T = 0$ K are summarized in Table 2, together with the available theoretical data. Generally speaking, although there are no experimental data, our computed results are consistent with the theoretical results obtained by Zhang et al. [26] and Ding et al. [30], using pseudopotential calculations. It can be also seen that C_{11} is very large compared to the other elastic constants, indicating that this compound is very incompressible under uniaxial stress along x (ε_{11}) axis. It was also found that C_{ij} constants of γ-CSi_2N_4 satisfy the

Table 2 The calculated elastic constants C_{ij} (in GPa), shear modulus G (in GPa), Young's modulus E (in GPa), Poisson's ratios σ, Lamé's coefficients $\mu$and λ (in GPa)

	C_{11}	C_{12}	C_{44}	B	G	E	σ	μ	λ	A	B/G
GGA	738.83	142.13	385.86	341.03	348.10	779.19	0.119	108.96	348.1	1.236	0.98
Ref. [26]	731.3	148.3	367.6	342.6	329.6	681.2	0.169			1.21	1.18
Ref. [30]	711.1	147.3	355.3	335.3	323.8	660.5	0.17				1.04

generalized criteria of mechanical stability for cubic crystals ($C_{11} - C_{12} > 0$, $C_{11} > 0$, $C_{44} > 0$, $C_{11} + 2C_{12} > 0$ [44].

The obtained values of the elastic moduli allow us to calculate the bulk B and shear G modulus. Two main approximations, namely, the Voigt (V) [45] and the Reuss (R) [46] are used to calculate the polycrystalline moduli. In cubic crystals, the bulk modulus can be determined in terms of the elastic constant of single crystal as:

$$B_V = B_R = (C_{11} + 2C_{12})/3,$$

where the shear moduli G_V and G_R have the following forms:

$$G_V = (C_{11} - C_{12} + 3C_{44})/5$$

and

$$G_R = 5(C_{11} - C_{12})C_{44}/[4C_{44} + 3(C_{11} - C_{12})]$$

The above elastic moduli C_{ij} were obtained from first-principles calculations for monocrystals but the majority of the synthesized materials is polycrystalline; i.e., in the form of aggregated mixtures of microcrystallines with random orientation. In such case, the Voigt–Reuss–Hill (VRH) approximation is widely used [47], where the actual effective moduli for polycrystals are expressed as the arithmetic mean of the two above mentioned limits—Voigt and Reuss:

$$B = \frac{B_V + B_R}{2}; \quad G = \frac{G_V + G_R}{2}$$

These values can be used also to determine the Poisson's ratio: $\sigma = (3B - 2G)/(6B + 2G)$, Young's modulus or modulus of elasticity (longitudinal), or constant linking the tensile stress (or compression) and the deformation of an isotropic material: $E = 9BG/(3B + G)$. Finally the Lame's constants μ, λcan be calculated easily by

$$\mu = \frac{E}{2(1+v)}; \quad \lambda = \frac{vE}{2(1+v)(1-2v)}.$$

The factor that measures the stability of a crystal against shear is the Poisson's ratio. Our calculated Poisson's ratio is given in Table 2. It is considerably smaller than the values reported for most of the intermetallic compounds. The smaller value of Poisson's ratio indicates that γ-CSi_2N_4 is relatively stable against shear. Poisson's ratio also provides more information for dealing with the characteristic of the bonding forces. For covalent materials σ is about 0.1, whereas the typical value of σ for ionic materials is about 0.25 [48]. In our case, the value of σ is 0.119, suggesting a high covalent contribution in intra-atomic bonding for this compound.

Poisson's ratio (σ) can also be used as a criterion for ductility or brittleness. According to Frantsevich rule [49], the critical value that separates the ductile and brittle nature of material is 0.26. For brittle materials, the Poisson's ratio is less than 0.26, otherwise the material behaves in a ductile manner. Here the calculated Poisson's value is smaller than (0.26), meaning that this compound is brittle in nature. Furthermore, according to Pugh criterion [50], the ratio of bulk modulus to shear modulus (B/G) of polycrystalline phases could also be used as metric to quantify whether a material would fail in a ductile or brittle manner. However, it is known that the bulk modulus B represents the resistance to fracture while the shear modulus G represents the resistance to plastic deformation. Subsequently, a high (low) value of this quotient is associated with ductility (brittleness). The critical value which separates the ductile and brittle was found to be 1.75. As mentioned in Table 2, this ratio is around 0.98, which also classifies this compound as a brittle material. Another index of ductility is the Cauchy's pressure, which is defined as the difference between the two particular elastic constants $C_{12} - C_{44}$ [51]. It is considered to serve as an indication of ductility. If the pressure is positive (negative), the material is expected to be ductile (brittle) [51]. Here the value of the Cauchy's pressure is found to be equal to −243.731 GPa, which clearly highlights the brittle nature of this compound. These results confirm the same observation established by different authors using pseudopotential method [6, 25, 26, 30]. The more deleterious consequence of brittleness is the sensitivity for thermal shocks, as the material cannot efficiently dissipate thermal stresses via plastic deformations. Thus, a brittle solid can only be subjected to limited thermal shocks before its strength drops dramatically. So we can conclude that the herein studied material is less sensitive to thermal shocks.

Mechanical anisotropy is yet another parameter to be considered, particularly in the indentation of single crystals [52]. It can provide us more information about possible appearance of microcrack in materials. To quantify this

quantity, we have computed the anisotropy factor $A = 2C_{44}/(C_{11} - C_{12})$ from the present values of the elastic constants [53]. The shear anisotropic factor may be obtained as a measure of the degree of anisotropy in the bonding between atoms in different planes. For a completely isotropic material, A is equal to 1, while any value smaller or larger than 1 indicates anisotropy. In our case, the calculated values of the anisotropic factor A are found to be equal to1.236, meaning that this compound has fairly low anisotropy. Another definition related to elastic anisotropy was emphasized by Chung and Buessem [54] as $A^* = (G_V - G_R)/(G_V + G_R)$, where G_V and G_R denote effective shear moduli calculated from the C_{ij} using Voigt or Reuss methods. For isotropic materials, $A^* = 0$ while in our case $A^* = 0.008$ clearly indicates that our material is nearly isotropic.

Electronic properties

In this section, we turn our attention to study the electronic properties of γ-CSi_2N_4 via calculating the energy band structure and the density of states. These are shown in Figs. 2 and 3. As shown in Fig. 2, the top of the valence band and bottom of the conduction band for γ-CSi_2N_4 are located at the Γ point, resulting in a direct band gap (Γ–Γ). The calculated band gap values for the herein studied compound using LDA, GGA, EV-GGA, and mBJ approximations are listed in Table 3, along with the available theoretical results [6, 26, 30] for comparison. From the results given in Table 3, it is clear that the obtained energy band gap values using the mBJ approach are higher than those obtained using LDA, GGA, and EV-GGA for the herein considered material. The calculated band gap values using GGA are in good agreement with those previously obtained [6, 26, 30] using the Vanderbilt ultrasoft pseudopotential and the linearized augmented plane wave methods. Since it is well known that DFT calculations within the common LDA and GGA severely underestimate the band gap values of spinel compounds [55], we can emphasize here that the present calculated band gap values using the mBJ approach for CSi_2N_4 compound are significantly improved.

To obtain a deeper insight into the electronic structure, we have also calculated the total and partial atomic densities of states (TDOS and PDOS) for γ-CSi_2N_4. Figure 3 shows the calculated TDOS and PDOS within only the

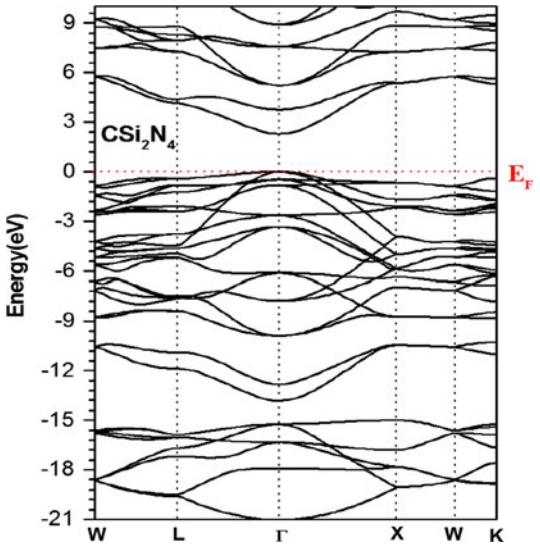

Fig. 2 TB-mBJ—electronic band dispersion curves of γ-CSi_2N_4 along some high symmetry directions of the Brillouin zone. The Fermi level is set to zero

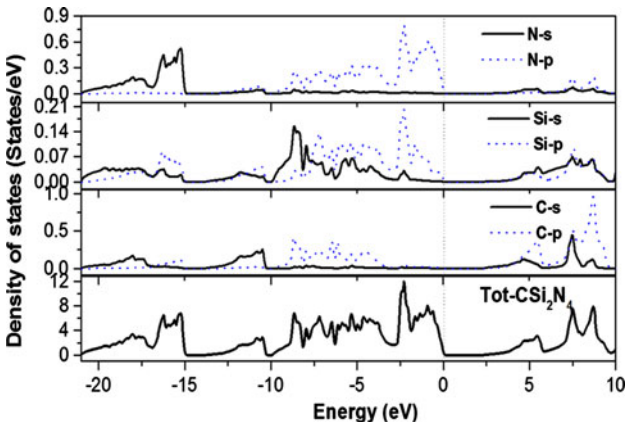

Fig. 3 TB-mBJ-total and partial densities of states ofγ-CSi_2N_4. The Fermi level is aligned to zero

Table 3 The calculated values of the main direct and indirect band gaps (Γ–Γ, Γ–L, Γ–X, Γ–K, Γ–W).

	Γ–Γ	L–L	X–X	K–K	W–W	Γ–L	Γ–X	Γ–K	Γ–W
LDA	1.63	3.69	5.08	4.80	5.84	3.24	4.41	4.39	4.85
GGA	1.46	3.54	4.90	4.64	5.61	3.14	4.30	4.28	4.71
EV-GGA	1.72	3.83	5.19	4.94	5.83	3.44	4.60	4.58	4.98
TB-mBJ	2.31	4.58	6.04	5.75	6.65	4.18	5.40	5.35	5.77
	1.74[a]								
	1.44[b]								
	1.34[c]								

All energies are (in eV)

[a] Ref. [26]

[b] Ref. [30]

[c] Ref. [6]

mBJ as a prototype since the pattern of the DOS is almost similar for all approximations. Following Fig. 3, we should emphasis that there are four distinct structures separated from each other's by gaps. Starting from the lower energy side, the deep structure situated between −20 and −15 eV, originates from N-*s* states with admixture of C and Si *s*/*p* states indicates the covalent bonding, which may explain the enhanced bulk modulus and hardness in the γ-CSi_2N_4 compound. The second structure lying between −13.0 and −10.0 eV consists entirely of C *p*-states. In the upside of valence band lying between −10.0 eV up to Fermi level, the bands are mainly N-*p* states with a few contribution from C-and Si-*p* states. The conduction bands are contributed mainly by the hybridization of *s* and *p* states of the cations and the N-*p* states.

In order to further explore the bonding nature in the cubic CSi_2N_4, the charge distribution in this compound is examined. The contour map of the charge density in (1 1 0) plane containing carbon (C), silicon (Si), and nitride (N) atoms is shown in Fig. 4. From the contour plot, it is clear that the bonding between C and N atoms is strong and the bonding between Si and N atoms is much weaker. This is a clear indication for the enhancement of the bulk modulus and the hardness in CSi_2N_4 compound. Furthermore, the charge transfer between cations and anions exists, which indicates an ionic contribution to the bonding. Thus, the bonding in CSi_2N_4 may be expressed as a mixture of covalent-ionic behavior.

Optical properties

All optical properties are calculated at the theoretical equilibrium lattice constant using the TB-mBJ approximation for the energy up to 40 eV. The real $\varepsilon_1(\omega)$ and imaginary $\varepsilon_2(\omega)$ parts of the dielectric function are illustrated in Fig. 5. The imaginary part $\varepsilon_2(\omega)$ of this function is directly related to the band structure of the material and describes its absorptive behavior. Here, we have calculated the optical properties for γ-CSi_2N_4 spinel structure and compared them with available theoretical data of Wang et al. [25] obtained using LAPW method within GGA approximation. We note that only direct transitions which conserve the crystal momentum are included in our optical property calculations. Indirect transitions such as those assisted by lattice vibrations are excluded and found to have very small effect on the absorption edge.

Our analysis of $\varepsilon_2(\omega)$ spectrum shows that the first critical point (threshold energy) of the dielectric function occurs at about 2.30 eV. This point is the direct optical transition between the highest valence band and the lowest conduction band at the γ-point. This is known as the fundamental absorption edge. Beyond this point, the curve increases rapidly due to the abruptly increase in the number of points contributing toward $\varepsilon_2(\omega)$. Wang et al. results showed that the most pronounced peak was located between 11.31 and 11.42 eV, which corresponds to the value of 12.58 eV in our results. This peak is probably related to the interband transition from occupied states with predominantly N-*p* character to hybridized unoccupied C-*p* and Si-*s* states. For the real part $\varepsilon_1(\omega)$ spectrum the main peak is located at about at 8.50 eV. The curve shows a decrease followed by an increase and then decreases to reach $\varepsilon_1(\omega)$ negative value; followed by a slow increase toward zero at high energy. The negative values of $\varepsilon_1(\omega)$ correspond to the local maxima of reflectivity as shown in Fig. 5c. The calculated static dielectric constant ε_1 (0) is found to be equal to 4.86, where Wang et al. reported a value of 5.83 using the same method. The difference between our calculated results and those of Wang et al.

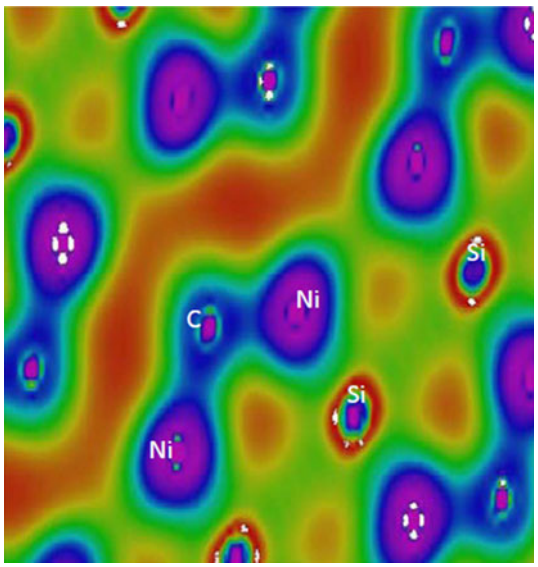

Fig. 4 2D contour plot for the total charge density of CSi_2N_4 in the (110) plane

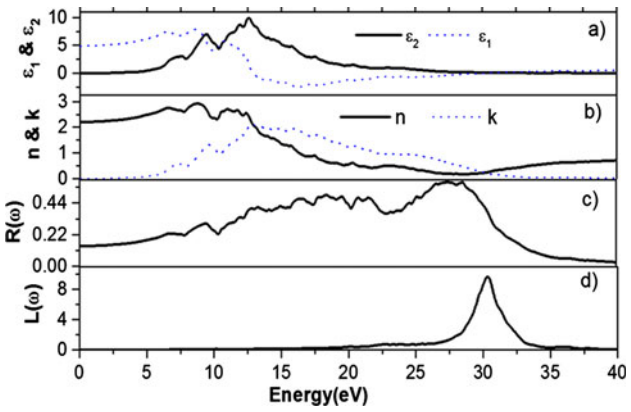

Fig. 5 (*a*) Real $\varepsilon_1(\omega)$ and imaginary $\varepsilon_2(\omega)$ parts, (*b*) refractive index $n(\omega)$ and extinction coefficient $k(\omega)$, (*c*) reflectivity $R(\omega)$ and (*d*) energy loss function $L(\omega)$ for γ-CSi_2N_4

[25] is due to the difference in the exchange and correlation (XC) potential.

The refractive index and the extinction coefficient are displayed in Fig. 5b. The static refractive index $n(0)$ is found to have the value 2.20. It increases with energy in the transparency region, reaching a peak in the ultraviolet at about 8.77 eV. It then decreases to a minimum level at 28.58 eV. The origin of the structures in the imaginary part of the dielectric function also explains the structures in the refractive index.

The variation of reflectance as a function of photon frequency $R(\omega)$ is displayed in Fig. 5c. The dynamic reflectance corresponds to the ratio of the intensities of the incident and reflected electric fields. In the low energy regime <7 eV the reflectance curves are nearly flat with reflectivity values of 0.17. The small value of reflectance ensures its applications as transparent coatings in the visible light regime. γ-CSi_2N_4 shows an overall larger reflectance in the range of 10–30 eV.

The electron energy loss function $L(\omega)$ is an important factor describing the energy loss of a fast electron traversing in a material. The prominent peaks in $L(\omega)$ spectra represent the characteristic associated with the plasma resonance (a collective oscillation of the valence electrons) and the corresponding frequency is the so-called plasma frequency ω_P. The peaks of $L(\omega)$ correspond to the trailing edges in the reflection spectra $R(\omega)$. For instance the prominent peak of $L(\omega)$ located at about 30.33 eV (Fig. 5d) is at an energy corresponding to the abrupt reduction of $R(\omega)$ (Fig. 5c).

Thermodynamic properties

The thermal behaviors of γ-CSi_2N_4 compound under high temperature and high pressure have been evaluated using the quasi-harmonic Debye approximation as implemented in Gibbs program. However, Debye model with quasi-harmonic approximation has its shortcomings: (i) it is applicable only for crystalline solid, (ii) it correctly predicts the low temperature dependence of thermal properties but due to simplifying assumptions, its accuracy suffers at intermediate temperatures when the system is no longer an ideal crystalline solid. In our case, the basic input parameters obtained from the energy–volume data are calculated using GGA-PBE and the thermal properties are determined in the temperature range from 0 to 2000 K where the quasi-harmonic model remains fully valid.

Figure 6 presents the normalized volume temperature diagram of γ-CSi_2N_4 at 0, 20, and 40 GP, obtained from the thermal EOS $V(P, T)$. The primitive cell volume increases with increasing temperature but the rate is more important for temperature range above 400 K. On the other side, as the pressure P increases, the relative volume V/V_0 decreases at a given temperature. One can also see that the rate of increase of the volume varies rapidly under lower pressure.

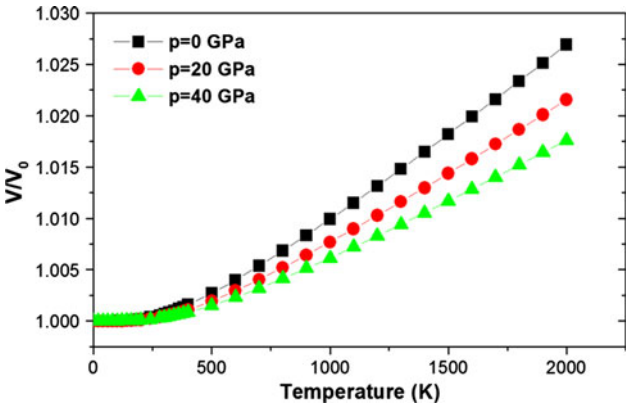

Fig. 6 The variation of the normalized volume with pressure and with temperature for γ-CSi_2N_4. V_0 is the equilibrium volume at $T = 0$ K

The relationship of the isothermal bulk modulus as a function of temperature at different pressure (0, 10, 20, 30, and 40 GPa) is shown in Fig. 7. For a given pressure, one can notice that the bulk modulus is nearly constant from 0 to 200 K and decreases linearly with increasing temperature for $T > 400$ K. The compressibility increases with increasing temperature at a given pressure and decreases with pressure at a given temperature. The above results are due to the fact that the effect of increasing pressure on the material is the same as that of the decreasing temperature. At zero pressure and temperature $T = 300$ K, the bulk modulus $B = 334$ GPa and $V = 96.86$ Å^3.

The variation of the heat capacities C_V versus temperature at 0.0, 20, and 40 GPa pressures is shown in Fig. 8. It is found that when $T < 1500$ K, the heat capacity C_V is depending on both temperature and pressure. At higher temperature ($T > 1500$ K) C_V tends to the Petit and Dulong limit, which

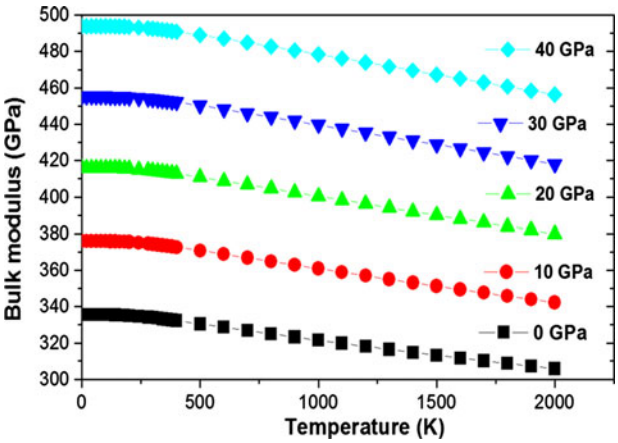

Fig. 7 The variation of the bulk modulus with temperature at some pressures of γ-CSi_2N_4

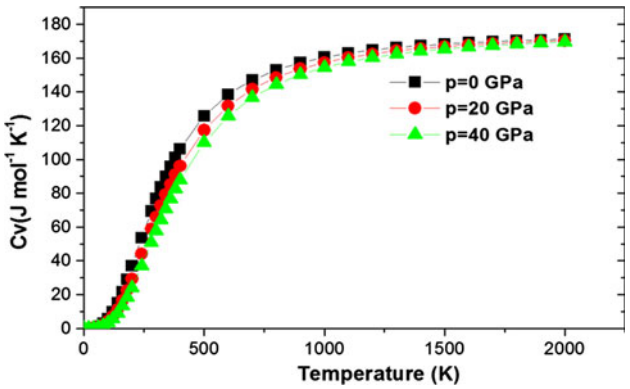

Fig. 8 The variation of the heat capacities C_V with temperature at some pressures of γ-CSi_2N_4

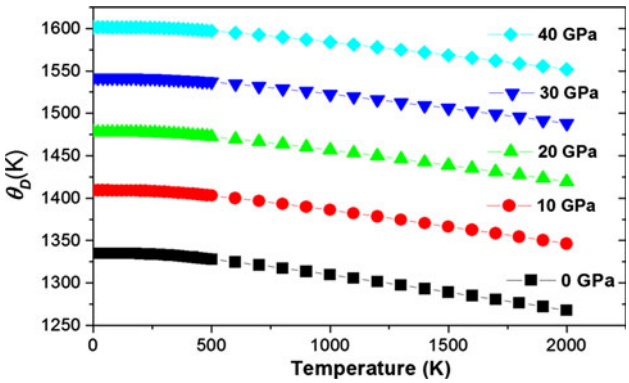

Fig. 10 The variation of the Debye temperature as a function of temperature at different pressures for γ-CSi_2N_4

is common to all solids at high temperature. At high temperature C_V approaches 170 Jmol^{-1} K^{-1}.

In Fig. 9, we present the effect of temperature on the thermal expansion coefficient (α). It is shown that the thermal expansion coefficient (α) increases with increasing temperature at a given pressure, the thermal coefficient α increases sharply with increasing the temperature up to 700 K. Above this temperature, α gradually approaches to a linear increasing with enhanced temperature. At zero pressure and 300 K, the thermal expansion α is 0.728334 $\times$ 10^{-5} K^{-1}.

The Debye temperature (θ_D) is an important parameter, characteristic for the thermal properties of solids. It is the temperature above which the crystal behaves classically, because the thermal vibrations become more important than the quantum effects. Figure 10 shows the evolution of θ_D with temperature at several fixed pressures. It can be seen that θ_D is nearly constant from 0 to 200 K and decreases linearly with increasing temperature. For a fixed temperature, the Debye temperature increases with the enhancement of pressure. Our calculated θ_D at zero pressure and ambient temperature is found to be equal to 1333 K. In this work, we obtained the Debye temperature θ_D equals to 1331.2 K at $P = 0$ GPa and $T = 0$ K. This value is somewhat greater than the value of 1131.74 K reported by Ding et al. [30] using GGA-PBE method. The discrepancy between the two results is due to different XC potentials used in each calculation.

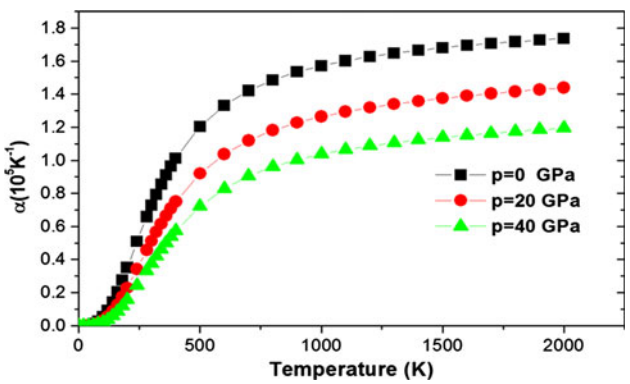

Fig. 9 The variation of the volume expansion coefficient α as function of temperature at some pressures for γ-CSi_2N_4

Conclusions

This study reports a detailed investigation on the structural, electronic, elastic, optical, and thermal properties of γ-CSi_2N_4 compound using first-principles APW + lo method within LDA, GGA, EV-GGA, and TB-mBJ potential. The most relevant conclusions are summarized as follows:

(1) The calculated ground state properties such as lattice parameters, bulk modulus and its pressure derivative agree quite well with the available theoretical results.
(2) The calculated ground state properties such as lattice parameters, bulk modulus and its pressure derivative agree quite well with the available theoretical results.
(3) The calculated elastic constants showed that γ-CSi_2N_4 is elastically stable where the computed Poisson rand B/G ratios clearly indicated that this spinel can be classified as brittle materials.
(4) The calculated band structure shows that the γ-CSi_2N_4 is a direct band gap material. However, we found that TB-mBJ yields larger band gaps compared to those calculated using LDA, GGA, and EV-GGA.
(5) Optical parameters such as the refraction index, dielectric constant, reflectivity, and the energy loss function are calculated and analyzed in this paper. The prominent variations in the optical parameters make γ-CSi_2N_4 suitable for optical devices.
(6) The quasi-harmonic Debye model is successfully applied to determine the thermal properties of γ-CSi_2N_4 in the 0–2000 K temperature range. Till now, there are no previous reports on the thermodynamic properties. We feel that our calculations can be used to cover the lack of data for this compound.

Acknowledgements Khenata, Bouhemadou, Alahmed, and Bin Omran acknowledge the financial support by the Deanship of Scientific Research at the King Saud University for funding the work through the research group Project No. RPG-VPP-088. The work of Khachai has been supported by the Algerian national research projects PNR (No. 8/0/627).

References

1. Zerr A, Riedel R, Sekine T, Lowther JE, Ching WY, Tanaka I (2006) Adv Mater (Weinheim, Germany) 18:2933 and references therein
2. Lowther JE (2011) Materials 4:1104
3. Ching WY, Rulis P (2006) Phys Rev B 73:045202 and references therein
4. Tanaka I, Oba F, Sekine T, Ito E, Kuba A, Tastumi K, Adach H, Yamamoto T (2002) J Mater Res 17:731
5. Mo SD, Ouyang LZ, Ching WY, Tanaka I, Koyama Y, Riedel R (1999) Phys Rev Lett 83:5046
6. Ching W-Y, Mo S-D, Ouyang L, Rulis P, Tanaka I, Yoshiya M (2002) J Am Ceram Soc 85:75
7. Zerr A, Schwarz M, Schmechel R, Kolb R, von Seggern H, Riedel R (2002) Acta Cryst A 58:C47
8. Leitch S, Moewes A, Ouyang L, Ching WY, Sekine T (2004) J Phys Condens Matter 16:6469
9. Zerr A, Miehe G, Serghiou G, Schwarz M, Kroke E, Riedel R, Fuess H, Kroll P, Boehler R (1999) Nature (London) 400:340
10. Zerr A, Scharz M, Serghiou G, Kroke E, Miehe G, Riedel R, Boehler R, Ger. Offen. (2000) DE 19855514 A1 (June, 8, 2000)
11. Jiang JZ, Kragh F, Frost DJ, Stahl K, Lindelov H (2001) J Phys. Condens Matter 13:L515
12. Jiang JZ, Lindelov H, Gerward L, Stahl K, Reico JM, Mori-Sanchez P, Carlson S, Mezouar M, Dooryhee E, Fitch A, Frost DJ (2002) Phys Rev B 65:161202
13. Jiang JZ, Ståhl K, Berg RW, Frost DJ, Zhou TJ, Shi PX (2000) Europhys Lett 51(1):62
14. Riedel R, Zerr A, Kroke E, Schwarz M (2001) Ceram Trans 112:119
15. Ching WY, Mo S-D, Ouyang LZ (2001) Phys Rev B 63:245110
16. Tanaka I, Oba F, Ching W-Y (2001) Mater Integr 14:21
17. Oba F, Tatsumi K, Adachi H, Tanaka I (2001) Appl Phys Lett 78:1577
18. Oba F, Tatsumi K, Tanaka I, Adachi H (2002) J Am Ceram Soc 85:97
19. Serghiou G, Miehe G, Tschauner O, Zerr A, Boehler R (1999) J Chem Phys 111:4659
20. Soignard E, McMillan PF (2004) Chem Mater 16:3533
21. Sekine T, He H, Kobayashi T, Zhang M, Xu F (2000) Appl Phys Lett 76:3706
22. He JL, Guo LC, Yu DL, Liu RP, Tian YJ, Wang HT (2004) Appl Phys Lett 85:5571
23. Ching WY, Mo SD, Tanaka I, Yoshiya M (2001) Phys Rev B 63:064102
24. Lowther JE, Amkreutz M, Frauenheim T, Kroke E, Riedel R (2003) Phys Rev B 68:033201
25. Wang H, Chen Y, Kaneta Y, Iwata S (2007) Eur Phys B 59:155
26. Zhang XY, Chen ZW, Du HJ, Yang C, Ma MZ, He JL, Tian YJ, Liu RP (2008) J Appl Phys 103:083533
27. Chang YK, Hsieh HH, Pong WF, Lee KH, Dann TE, Chien FZ, Tseng PK, Tsang KL, Su WK, Chen LC, Wei SL, Chen KH, Bhusari DM, Chen YF (1998) Phys Rev B 58:9018
28. Badzian A (2002) J Am Ceram Soc 85:16
29. Kroll P, Riedel R, Hoffman R (1999) Phys Rev B 60:3126
30. Ding Y-C, Chen M, Jiang M-H, Gao X-Y (2012) Phys B Condens Matter 407:4323
31. Sjöstedt E, Nordström L, Singh DJ (2000) Solid State Commun 114:15
32. Wong KM, Alay-e-Abbas SM, Shaukat A, Fang Y, Lei Y (2013) J Appl Phys 113:014304
33. Wong KM, Alay-e-Abbas SM, Fang Y, Shaukat A, Lei Y (2013) J Appl Phys 114:034901
34. Blaha P, Schwarz K, Madsen GKH, Kvasnicka D, Luitz J (2001) WIEN2k: an augmented plane wave + local orbitals program for calculating crystal properties. Karlheinz Schwarz/Techn. Universität Wien, Wien
35. Engel E, Vosko SH (1993) Phys Rev B 47:13164
36. Tran F, Blaha P (2009) Rev Lett 102:226401
37. Monkhorst HJ, Pack JD (1976) Phys Rev B 13:5188
38. Ambrosch-Draxl C, Sofo JO (2006) Comput Phys Commun 175:1
39. Delin A, Eriksson AO, Ahuja R, Johansson B, Brooks MSS, Gasche T, Auluck S, Wills JM (1996) Phys Rev B 54:1673
40. Yu YP, Cardona M (1999) Fundamental of semiconductors physics and materials properties, 2nd edn. Springer, Berlin, p 233
41. Blanco MA, Francisco E, Luaña V (2004) Comput Phys Commun 185:57
42. Murnaghan FD (1944) Proc Natl Acad Sci USA 30:244
43. Mehl MJ (1993) Phys Rev B 47:2493
44. Wallace DC (1972) Thermodynamics of crystals. Wiley, New York
45. Hill R (1952) Proc Phys Soc Lond A 65:349
46. Voigt W (1928) Lehrbuch der Kristallphysik. Teubner, Leipzig
47. Russ A, Angew A (1929) Math Phys 9:49
48. Ravindran P, Fast L, Korzhavyi PA, Johansson B, Wills J, Eriksson O (1990) J Appl Phys 84:4891
49. Frantsevich IN, Voronov FF, Bokuta SA (1983) Elastic constants and elastic moduli of metals and insulators: Handbook. In: Frantsevich IN (ed), Naukova Dumka, Kiev, p 60–180
50. Pugh SF (1954) Philos Mag 45:823
51. Pettifor DG (1992) Mater Sci Technol 8:345
52. Lawn BR, Wilshaw TR (1975) J Mater Sci 10:1049. doi:10.1007/BF00823224
53. Zener C (1948) Elasticity and anelasticity of metals. University of Chicago Press, Chicago, p 16
54. Chung D, Buessem W (1967) J Appl Phys 38:2010
55. Scanlon DO, Watson GW (2011) Phys Chem Chem Phys 13:9667